

# Matter-wave solitons supported by field-induced dipole-dipole repulsion with a spatially modulated strength

Yongyao Li<sup>1,2,3</sup>, Jingfeng Liu<sup>1</sup>, Wei Pang<sup>4</sup>, and Boris A. Malomed<sup>2\*</sup>

<sup>1</sup>*Department of Applied Physics, South China Agricultural University, Guangzhou 510642, China*

<sup>2</sup>*Department of Physical Electronics, School of Electrical Engineering,  
Faculty of Engineering, Tel Aviv University, Tel Aviv 69978, Israel*

<sup>3</sup>*Modern Educational Technology Center, South China Agricultural University, Guangzhou 510642, China*

<sup>4</sup>*Department of Experiment Teaching, Guangdong University of Technology, Guangzhou 510006, China.*

We demonstrate the existence of one and two-dimensional *bright* solitons in the Bose-Einstein condensate with *repulsive* dipole-dipole interactions induced by a combination of dc and ac polarizing fields, oriented perpendicular to the plane in which the BEC is trapped, assuming that the strength of the fields grows in the radial ( $r$ ) direction faster than  $r^3$ . Stable tightly confined 1D and 2D fundamental solitons, twisted solitons in 1D, and solitary vortices in 2D are found in a numerical form. The fundamental solitons remain robust under the action of an expulsive potential, which is induced by the interaction of the dipoles with the polarizing field. The confinement and scaling properties of the soliton families are explained analytically. The Thomas-Fermi approximation is elaborated for fundamental solitons. The mobility of the fundamental solitons is limited to the central area. Stable 1D even and odd solitons are also found in the setting with a double-well modulation function, along with a regime of Josephson oscillations.

PACS numbers: 03.75.Lm; 42.65.Tg; 47.20.Ky; 05.45.Yv

## I. INTRODUCTION AND THE SETTING

The transition of ultracold dipolar atomic gases into the Bose-Einstein condensate (BEC) has been demonstrated in chromium [1, 2], dysprosium [3], and erbium [4]. Also promising for experiments in this direction is the use of CO [5], ND<sub>3</sub> [6], and OH [7, 8] molecular gases. Unlike the usual contact nonlinearity, which represents effects of collisions between atoms, dipole-dipole interactions (DDIs) give rise to long-range anisotropic forces. The DDIs account for a number of remarkable phenomena in ultracold Bose gases [9]-[11], such as various pattern-formation scenarios [12–16], fractional domain walls [17],  $d$ -wave collapse [18, 19], specific possibilities for precision measurements [20–22], stabilization of the dipolar BEC by optical lattices [23, 24], the Einstein - de Haas effect [25], *etc.* Dipolar BECs can be also used as *matter-wave simulators* [26], to emulate, in particular, the creation of multi-dimensional solitons via the nonlocal nonlinearity—a subject which has also drawn much attention in optics, where nonlocal interactions of other types (with different interaction kernels) occur too [27–29]. In fact, the dipolar condensates not only emulate the situation known in optics, but also make it possible to predict the existence of solitons with novel properties. Recently, one- and two-dimensional (1D and 2D) fundamental and vortical solitons in dipolar BEC have been predicted in various continuous and discrete settings [24, 30–40]. A similar mechanism can create 1D solitons in the Tonks-Girardeau gas with attractive DDIs between particles [41].

The formation of bright solitons, which was previously demonstrated in BEC experimentally [42], and studied in detail theoretically [43, 44], requires the presence of self-attraction. However, in models with local interactions it has been recently demonstrated that *bright* solitons may be supported by the *repulsive* cubic nonlinearity in the  $D$ -dimensional geometry, provided that the nonlinearity strength is modulated in space, growing from the center to periphery at any rate faster than  $R^D$ , where  $R$  is the radial coordinate [45]-[48]. A similar result was obtained for the local self-repulsive quintic nonlinearity, in which case the nonlinearity strength must grow faster than  $r^{2D}$  [49]. A generalization for bright solitons in the 1D optical model with a self-defocusing nonlocal thermal nonlinearity, whose strength grows at  $|x| \rightarrow \infty$  through the corresponding modulation of the density of absorbing dopants, was very recently elaborated in Ref. [50].

The use of the spatially profiled repulsive nonlinearities for the creation of multidimensional solitons is more than an exploration of an exotic possibility. Indeed, 2D and 3D solitons supported by usual self-attractive cubic terms are subject to the instability against the critical or supercritical collapse, which makes their stabilization a great challenge

---

\*Electronic address: malomed@post.tau.ac.il

[51]. In the case of self-repulsion, the collapse is ruled out—in fact, the fundamental 2D solitons and simplest vortices are automatically stable in that case, if they exist [45]-[48].

The subject of the present work is to predict the creation of stable bright solitons in nearly-2D or 1D dipolar condensates, which are trapped, respectively (by means of an appropriate optical potential), in a thin layer close to  $z = 0$  (or in a “cigar” around axis  $x$ ), with the local strength of the *repulsive* DDI growing fast enough at  $r \equiv \sqrt{x^2 + y^2} \rightarrow \infty$  (or at  $|x| \rightarrow \infty$ ). This situation can be implemented in the case when the atoms or molecules do not carry permanent electric or magnetic dipole moments, but rather ones induced by external electric or magnetic field [52]-[56]. To the best of our knowledge, the formation of solitons or other nonlinear modes in the gas of dipoles induced by inhomogeneous external fields was not investigated previously in any setting.

We consider a combination of dc and ac external fields directed along the  $z$  direction:

$$\mathbf{G}(r) = F(r) [f_{\text{dc}} + f_{\text{ac}} \cos(\omega t)] \mathbf{e}_z. \quad (1)$$

Then, the local dipolar moment  $\mathbf{g} = g(t)\mathbf{e}_z$  of the atom or molecule is determined by the intrinsic equation of motion, considered here in the classical approximation [57]:

$$\ddot{g} + \omega_0^2 g + \gamma \dot{g} = F(r) [\lambda(0)f_{\text{dc}} + \lambda(\omega)f_{\text{ac}} \cos(\omega t)], \quad (2)$$

where  $\omega_0$  is the intrinsic eigenfrequency and  $\gamma$  is the damping coefficient,  $\lambda(0)$  and  $\lambda(\omega)$  being effective static and dynamical susceptibilities. We will also consider a model combining permanent and induced moments, see Eq. (21) below.

In the off-resonance situation, when ac frequency,  $\omega$ , is not too close to  $\omega_0$ , the small dissipative term in Eq. (2) may be neglected, which gives rise to an obvious solution,

$$g_{\text{off}}(r, t) = F(r) \left[ \frac{\lambda(0)}{\omega_0^2} f_{\text{dc}} + \frac{\lambda(\omega)}{\omega_0^2 - \omega^2} f_{\text{ac}} \cos(\omega t) \right]. \quad (3)$$

On the other hand, the ac drive close to the resonance yields

$$g_{\text{res}}(r, t) = \frac{\lambda(\omega_0)}{\gamma \omega_0} F(r) \sin(\omega_0 t). \quad (4)$$

These results lead to the following time-averaged DDI strengths,

$$\langle g_{\text{off}}(r_1, t) g_{\text{off}}(r_2, t) \rangle = F(r_1) F(r_2) \left[ \frac{\lambda^2(0)}{\omega_0^4} f_{\text{dc}}^2 + \frac{\lambda^2(\omega)}{2(\omega_0^2 - \omega^2)^2} f_{\text{ac}}^2 \right], \quad (5)$$

$$\langle g_{\text{res}}(r_1, t) g_{\text{res}}(r_2, t) \rangle = F(r_1) F(r_2) \frac{\lambda^2(\omega_0)}{2\gamma^2 \omega_0^2}. \quad (6)$$

In addition to the DDIs, in the off-resonance situation the field-induced dipole moments give rise to the effective averaged potential of the dipole-field interaction:

$$V(r) = -\langle \mathbf{g}_{\text{off}} \cdot \mathbf{G} \rangle = -F^2(r) \left[ \frac{\lambda(0)}{\omega_0^2} f_{\text{dc}}^2 + \frac{\lambda(\omega)}{2(\omega_0^2 - \omega^2)} f_{\text{ac}}^2 \right] \equiv -\chi F^2(r), \quad (7)$$

where  $\chi$  is the effective average polarizability. On the contrary, in the resonant situation the substitution of expression (4) yields  $V(r) = 0$ . With the spatially growing modulation function  $F(r)$ , potential (7) is *expulsive* ( $\chi > 0$ ), at  $\omega^2 < \Omega^2$ , with  $\Omega^2$  defined by equation

$$\frac{\Omega^2}{\omega_0^2} = 1 + \frac{\lambda(\Omega)}{2\lambda(0)} \frac{f_{\text{ac}}^2}{f_{\text{dc}}^2}, \quad (8)$$

and trapping ( $\chi < 0$ ) at  $\omega^2 > \Omega^2$ . Obviously, the expulsive potential (EP) hampers the possibility of inducing self-trapping of localized modes, while the trapping one makes it rather trivial. Below, we chiefly focus on the setting with the self-trapping determined by the DDIs in the “pure” form, when EP (7) vanishes. This may correspond to  $\omega = \Omega$ , or to the resonance,  $\omega = \omega_0$ , see above. Nevertheless, it will also be demonstrated that the spatially modulated DDI may support the self-trapping even in the presence of EP (7), provided that its strength is weak enough.

The electric field subject to the appropriate spatial modulation may be created by charged grids forming a lens-like capacitor, as shown in Fig. 1. Such capacitors can be built using techniques developed for ion-holding microtraps

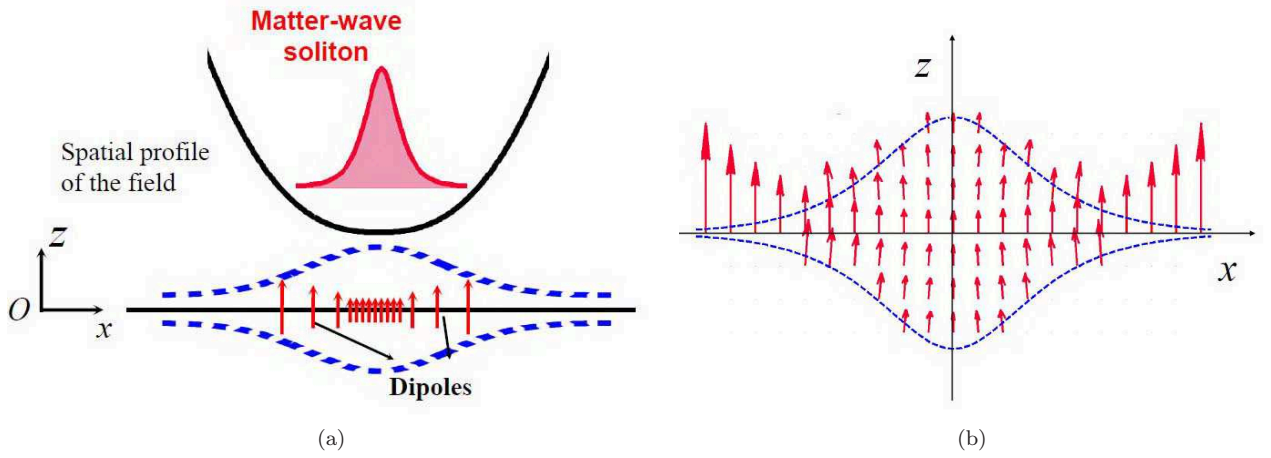


FIG. 1: (Color online) (a) The setting for the condensate trapped in the  $(x, y)$  plane. The polarizing field, with the strength increasing along the radial coordinate,  $r = \sqrt{x^2 + y^2}$ , is directed parallel to the  $z$ -axis, inducing the local dipole moments oriented in the same direction. The dashed curves designate lens-shaped charged grids (electrodes), which may create the necessary electrostatic field, such as the one given by Eq. (9). In the latter case, the shape of the electrodes is determined by Eq. (10), and the full distribution of the electrostatic field  $\mathbf{E}^{(2D)}$ , as given by Eq. (9), is displayed in panel (b), in the plane of  $y = 0$  (the scale is arbitrary).

[58, 59]. In particular, suitable separable solutions of the wave equation for the ac electric field ( $\omega \neq 0$ ), or Laplace equation for the dc field ( $\omega = 0$ ) are

$$\left\{ \begin{array}{l} E_z^{(2D)}(x, z) \\ E_z^{(1D)}(r, z) \end{array} \right\} = E_0 \left\{ \begin{array}{l} \cos\left(\sqrt{1/x_0^2 + \omega^2/c_0^2}z\right) I_0(r/x_0) \\ \cos\left(\sqrt{1/x_0^2 + \omega^2/c_0^2}z\right) \cosh(x/x_0), \end{array} \right\} \cos(\omega t) \quad (9)$$

for the nearly-2D and 1D condensates. Here,  $E_0$  is the field amplitude,  $x_0$  is an arbitrary length scale,  $c_0$  is the light velocity in vacuum, and  $I_0$  is the modified Bessel function. The shape of the electrodes creating such dc fields is determined by respective equipotential surfaces:

$$\sin(z/x_0) = \pm \frac{1}{2}U \left\{ \begin{array}{l} [I_0(r/x_0)]^{-1}, \text{ in 2D,} \\ \text{sech}(x/x_0), \text{ in 1D,} \end{array} \right. \quad (10)$$

where  $U$  is the voltage applied to the capacitor. Equation (10) demonstrates that, for a given modulation scale  $x_0$  (a natural range of values is  $x_0 \sim 10 \mu\text{m}$ ), the distance between the electrodes may be made large enough, if this is required by the design of the experimental setup. On the other hand, it is relevant to mention that available technologies make it possible to build capacitors with the separation between the electrodes  $\sim$  a few  $\mu\text{m}$ , while the lateral size of the capacitor may be measured in hundreds of  $\mu\text{m}$  [60].

The time-averaged potential of the DDI between two dipole moments,  $g_1$  and  $g_2$ , placed at positions  $\mathbf{r}_1$  and  $\mathbf{r}_2$ , is

$$V_{\text{dd}}(\mathbf{R}_{12}) = C_{\text{dd}} \frac{\langle \mathbf{g}_1(r_1) \cdot \mathbf{g}_2(r_2) \rangle r_{12}^2 - 3 \langle (\mathbf{g}_1(r_1) \cdot \mathbf{r}_{12})(\mathbf{g}_2(r_2) \cdot \mathbf{r}_{12}) \rangle}{r_{12}^5}, \quad (11)$$

where  $r_{12} = |\mathbf{r}_1 - \mathbf{r}_2|$ , the time averaging,  $\langle \dots \rangle$ , is realized as in Eqs. (5) and (6), and  $C_{\text{dd}} = 1/(4\pi\epsilon_0)$  or  $C_{\text{dd}} = \mu_0/4\pi$  for the electric and magnetic dipole moments, respectively. Because the dipole moments in the setting displayed in Fig. 1 are parallel to the  $z$  axis, and the condensate is confined to the  $(x, y)$  plane, expression (11) simplifies to  $V_{\text{dd}} = C_{\text{dd}} \langle g_1(r_1)g_2(r_2) \rangle / r_{12}^3$ . In the mean-field approximation, the Hamiltonian of this 2D setting is [10]

$$H = \frac{\hbar^2}{2m} \int d\mathbf{r} |\nabla\psi(\mathbf{r})|^2 + \frac{1}{2}C_{\text{dd}} \int \int d\mathbf{r} d\mathbf{r}' f(\mathbf{r} - \mathbf{r}') g(r) |\psi(\mathbf{r})|^2 g(r') |\psi(\mathbf{r}')|^2 - \chi \int d\mathbf{r} F^2(r) |\psi(\mathbf{r})|^2, \quad (12)$$

where  $\psi(\mathbf{r})$  is the single-particle wave function,  $m$  is the mass of the particle,  $\chi$  is the strength of EP (7) (if it is present), and the kernel in the integral term is taken as

$$f(\mathbf{r} - \mathbf{r}') = (\epsilon^2 + |\mathbf{r} - \mathbf{r}'|^2)^{-3/2}, \quad (13)$$

where the regularization scale  $\varepsilon$  is provided by the thickness of the confined layer in the  $z$  direction. The scaled Gross-Pitaevskii equation (GPE), Eq. (19), is written below so that  $x = 1$  corresponds to physical distance  $\sim 10 \mu\text{m}$ . Accordingly, we set  $\varepsilon = 0.1$  in Eq. (13). We do not include local (contact) interactions here, to focus on the possibility of inducing the self-trapping solely by means of the spatially modulated *repulsive* DDI.

Hamiltonian (12) gives rise to the 2D nonlocal GPE,

$$i \frac{\partial \psi(\mathbf{r})}{\partial t} = -\frac{\hbar^2 \nabla^2}{2m} \psi(\mathbf{r}) + C_{\text{dd}} g(\mathbf{r}) \psi(\mathbf{r}) \int d\mathbf{r}' f(\mathbf{r} - \mathbf{r}') g(\mathbf{r}') |\psi(\mathbf{r}')|^2 - \chi F^2(r) \psi(\mathbf{r}). \quad (14)$$

Obviously, Eq. (14) has three dynamical invariants, namely the Hamiltonian, the total number of particles, which is proportional to the norm of the wave function,

$$P = \int |\psi(\mathbf{r})|^2 d\mathbf{r}, \quad (15)$$

and the  $z$ -component of the angular momentum,

$$M = i \int \psi^* (y\psi_x - x\psi_y) d\mathbf{r}, \quad (16)$$

where  $\psi^*$  stands for the complex conjugate.

As shown in Fig. 1, the magnitude of the polarizing field grows at  $r \rightarrow \infty$ , which results in a growing local value of the dipole moment. With the repulsive DDI, fundamental and vortical solitons may self-trap in a finite isotropic area around the center, due to the greater strength of the DDI-mediated repulsion in the outer area. The 1D version of the system is described by the obvious 1D reduction of Eqs. (14) and (13).

In reality, the indefinite growth of the polarizing field at  $r \rightarrow \infty$  is not necessary. As shown below, solitons emerging in such settings are well localized modes, hence the supporting profile of the external field should be actually created in a finite area, as the presence of the field at large distances from the center, to which the soliton extends no tangible tail, is not needed. The same argument is relevant as concerns the possible presence of EP (7). Formally speaking, trapped modes cannot exist in the presence of the expulsive potential which indefinitely grows at  $r \rightarrow \infty$ . However, as is shown below, the system considered in a finite area of a reasonably large size may readily overcome the destructive effect of the EP.

Thus, our objective is to demonstrate the self-trapping of localized modes (of the fundamental and vortical types alike) in the present model via the action of the repulsive DDI, assuming that the local dipole moments are induced by the external field according to Eq. (1), with the field growing from the center to periphery as  $r^\alpha$ . As we demonstrate below analytically, an important difference of the present nonlocal model from its local counterparts [45]-[49] is tight *super-exponential* localization of the solitons, see Eq. (23) below, in contrast with the loose (power-law) localization in the local models, which is determined by the Thomas-Fermi approximation (TFA) [45],

$$|\psi(r)|^2 \sim r^{-\alpha}. \quad (17)$$

Obviously, the sharp localization should help to observe solitons in the experiment.

Another significant difference is that the minimum value of the growth rate  $\alpha$ , above which normalizable self-trapped modes exist in the present model, is  $\alpha_{\text{min}}^{(\text{dd})} = 3$ , and it does not depend on spatial dimension  $D$ , see Eq. (24) below (we actually use  $\alpha = 4$ ), unlike the above-mentioned minimum value in the local model with the cubic nonlinearity:

$$\alpha > \alpha_{\text{min}}^{(\text{local})} = D, \quad (18)$$

which actually follows from Eq. (17) [45]. Also drastically different from the local model are scalings which characterize dependences between the solitons' norm and chemical potential, as Eqs. (27) and (28) demonstrate in the following sections.

To estimate a range of physical parameters relevant to the setting considered here, we note that the intrinsic nonlinearity, induced by the magnetic [9] or electric [61] DDIs, may be roughly estimated as the contact interaction with an effective scattering length,  $a_s \sim mg^2/\hbar^2$ . With characteristic values of the molecular electric polarizability relevant to experiments with ultracold gases,  $\chi \sim 100 \text{ \AA}^3$  [62], and the corresponding molecular weight,  $\sim 100$ , the magnitude of the effective scattering length sufficient for the formation of localized modes,  $a_s \sim 0.1 \text{ nm}$  [42], may be emulated by the polarizing dc electric field in a range of  $E \sim 10 \text{ kV/cm}$ , which is definitely accessible to the experiment. Further, results for the 1D and 2D settings, presented in Figs. 3 and 6, respectively, along with the modulation profile (21) adopted below, demonstrate that, within the area of the actual localization of the solitons,

the field increases from the center to periphery by a factor  $\lesssim 20$ , which is compatible with the above-mentioned range of the values of  $E$ . Because the density of the condensate is very low ( $\sim 10^{15} \text{ cm}^{-3}$ , in the most typical case), and the contact of molecules with the field-inducing grids is prevented by the optical trap, see Fig. 1, the electric breakdown of the low-density gas is not a severe danger either in this setting.

As concerns the role of EP (7), an estimate suggests that it can be made negligible in comparison with the DDI, in the region where the self-trapped mode is localized, if the condensate density is raised to values  $\sim 10^{18} \text{ cm}^{-3}$  (then, the number of molecules expected in the nearly-1D soliton will be  $\sim 10^6$ , instead of the most typical value  $\sim 10^3$  [42]). Alternatively, the same result may be achieved by bringing the ac drive to a proximity of the resonance with the relative detuning  $|\omega_0 - \omega|/\omega_0 \sim 10^{-3}$ , see Eq. (2).

Lastly, it is relevant to mention that a similar situation may be expected in BEC with long-range interactions induced by the resonant laser illumination [63]. However, the consideration of that setting is beyond the scope of the present work.

The rest of the paper is structured as follows. In Sec. II, analytical and numerical results are reported for basic types of stable self-trapped modes which can be supported by the spatially growing nonlocal repulsion, namely, 1D and 2D fundamental solitons, twisted (spatially odd) modes in 1D, and solitary vortices in 2D. The phenomenology of the soliton modes is summarized by means of dependences of their chemical potentials and spatial size on the norm. In most cases, these dependences can be explained by means of a simple analysis of scaling in Eq. (19) (with  $\chi = 0$ ). Stability of the modes in the presence of EP (7) is considered too, as well as the TFA for the 1D and 2D fundamental solitons. In Sec. III, motion of shifted and/or kicked 1D and 2D fundamental solitons around the center is considered. In Sec. IV, we change the 1D setting from the single-well modulation of the polarizing field to a double-well configuration, and study properties of solitons in that case (configurations of this type were not studied previously even in models which maintain bright solitons by means of the spatially growing local repulsive nonlinearity). The paper is concluded by Sec. V.

## II. SOLITONS SUPPORTED BY THE FIELD-INDUCED REPULSIVE DIPOLE-DIPOLE INTERACTION

### A. Analytical considerations

Stationary solutions to Eq. (14) with chemical potential  $\mu$  are looked for as  $\psi(t, \mathbf{r}) = e^{-i\mu t} \phi(\mathbf{r})$ . Setting, by means of an obvious rescaling,  $\hbar = m = C_{\text{dd}} = 1$ , and, as said above, scaling the distances so that  $x = 1$  corresponds to physical length  $\sim 10 \mu\text{m}$ , the corresponding equation for the (generally, complex) stationary wave function  $\phi$  is derived in the following form:

$$\mu\phi(\mathbf{r}) + \frac{1}{2m}\nabla^2\phi(\mathbf{r}) - g(\mathbf{r})\phi(\mathbf{r}) - \int d\mathbf{r}' f(\mathbf{r} - \mathbf{r}')g(\mathbf{r}')|\phi(\mathbf{r}')|^2 + \chi F^2(r)\phi(\mathbf{r}) = 0. \quad (19)$$

As said here, we chiefly solved Eq. (19) with  $m = 1$ , but coefficient  $m$  is kept as a free one for the consideration of the TFA (see below), which corresponds to dropping the kinetic-energy term in the equation, i.e., setting  $m \rightarrow \infty$ . The above-mentioned physical estimates imply that values  $P \sim 1$  of the scaled norm (15) correspond to the numbers of particles  $N \sim 10^3$  and  $10^4$  in the 1D and 2D solitons displayed below, see Figs. 3 and 6.

Multiplying Eq. (19) by  $\phi^*(\mathbf{r})$  and integrating the result over the space, it is easy to prove that the equation may give rise to localized solutions only with  $\mu > 0$  (this proof is similar to that in the model with the spatially modulated strength of the local self-repulsive nonlinearity [46]), while the usual bright solitons, in the uniform space with self-attractive nonlinearities, always have  $\mu < 0$ .

The tightness of self-trapping of the 2D modes is characterized by their effective area,

$$A_{\text{eff}} = P^2 \left( \int |\phi(\mathbf{r})|^4 d\mathbf{r} \right)^{-1}, \quad (20)$$

where  $P$  is the norm introduced in Eq. (15). The 1D counterpart of  $A_{\text{eff}}$  measures the effective width of the 1D mode.

To introduce the spatial modulation of the local dipole moment, we assume that the strength of the polarizing field and, accordingly, the local moment [see Eqs. (3) and (4)] grow with  $r$  as

$$g(r) = r^\alpha + g_0, \quad (21)$$

with  $g_0 \geq 0$ . Two interpretations of this modulation profile are possible: (i) the constant term,  $g_0$ , may be a permanent part of the particle's dipole moment, while  $r^\alpha$  is, in the appropriately scaled notation, the addition induced by the

external field whose strength grows as  $r^\alpha$ , or (ii) the field profile is patterned as in Eq. (21), the entire dipole moment being induced by the field.

Solitons with a convergent norm exist if the growth rate  $\alpha$  in Eq. (21) exceeds a certain critical value,  $\alpha_{\min}$ . In the local model with the strength of the cubic self-repulsive term growing as  $r^\alpha$ , the TFA [see Eq. (17)] readily demonstrates that the self-trapped modes are normalizable for  $\alpha > D$ , as stated in Eq. (18). In fact, this result is an exact one, which is not predicated on the validity of the TFA [45].

In the present nonlocal model, another approximation makes it possible to identify  $\alpha_{\min}$ . Indeed, assuming that the soliton is represented by an axisymmetric localized solution of Eq. (19),  $\phi(r)$ , or by its 1D counterpart  $\phi(x)$ , in the limit of  $r \rightarrow \infty$  (or  $|x| \rightarrow \infty$ , at  $D = 1$ ), the asymptotic form of Eqs. (19), (21) and (13) with  $\chi = 0$  yields

$$\frac{d^2\phi}{dr^2} + \frac{D-1}{r} \frac{d\phi}{dr} + 2\mu\phi - 4r^{\alpha-3}\phi(r) \int_0^\infty |\phi(r')|^2 g(r') (\pi r')^{D-1} dr' = 0. \quad (22)$$

For  $\alpha > 3$ , Eq. (22) takes the form of the 1D linear Schrödinger equation, with coordinate  $r$ , and an effective potential growing as  $r^{\alpha-3}$ . Accordingly, the asymptotic form of the relevant solution to this equation is

$$\phi(r) = \phi_0 \exp\left(-\frac{4\sqrt{Q_D}}{\alpha-1} r^{\frac{\alpha-1}{2}}\right), \quad (23)$$

where constants  $\phi_0$  and  $Q_D \equiv \int_0^\infty \phi^2(r)g(r) (\pi r')^{D-1} dr$  are characteristics of the corresponding global solution. Thus, at

$$\alpha > \alpha_{\min}^{(dd)} = 3, \quad (24)$$

the super-exponentially localized self-trapped states exist for either dimension,  $D = 1$  or  $2$ . Furthermore, an analysis of Eq. (19), with regard to Eqs. (21) and (13), suggests that, at  $\alpha > 3$ , the solitons exist for all values of norm (15). In particular, at  $P \rightarrow 0$  the soliton becomes broad, and Eq. (19) gives rise to the following scaling relations between  $P$ , peak density  $\phi_0^2$ , and a characteristic radial size of the soliton,  $r_0$ :

$$r_0 \sim P^{-\frac{1}{2\alpha-1}}, \quad \phi_0^2 \sim P^{\frac{2\alpha+D-1}{2\alpha-1}}. \quad (25)$$

On the other hand, at  $\alpha < 3$  Eq. (22) simplifies, in the lowest approximation, to  $\phi'' + 2\mu\phi = 0$ , which, obviously, cannot have localized solutions with  $\mu > 0$ . Detailed analysis of the critical case,  $\alpha = 3$ , is beyond the scope of the present work. Below, we report numerical results with  $\alpha = 4$ , for  $D = 1$  and  $2$  alike.

## B. One-dimensional solitons

The numerical solution of the 1D version of Eq. (19) with

$$g(x) = x^4 + g_0 \quad (26)$$

was carried out by means of numerical code PCSOM elaborated in Refs. [64, 65]. First, in Fig. 2 we present basic results obtained in the model including EP (7) with strength  $\chi$ . Panel (a) demonstrates that, if  $\chi$  is not small enough, the EP generates a nonvanishing tail, which breaks the self-trapped character of the mode. For the same case, panel 2(c) shows that the presence of the EP makes the soliton unstable in direct simulations, which were performed by adding small random perturbations to the initial configuration. The instability is, naturally, still stronger for a smaller value of the norm, as shown in panel 2(b). On the other hand, the increase of the norm makes the soliton robust due to the stronger nonlinearity, in accordance with the estimate given at the end of Section I.

Next, we report the results obtained in the basic model with  $\chi = 0$ , to which the more general one may be reduced as discussed in Section I. In this case, the numerical solution of the 1D version of Eq. (19) produces families of fundamental (spatially even) and twisted (odd) solitons. Typical examples are displayed in Fig. 3 [higher-order (*multipole*) localized 1D modes can be easily found too]. In particular, Figs. 3(c) and 3(g) show that the soliton families satisfy the so-called anti-Vakhitov-Kolokolov criterion,  $d\mu/dP > 0$ , which plays the role of a necessary stability condition for bright solitons in self-repulsive media [66]. Indeed, direct simulations of the perturbed evolution of the solitons, performed in the framework of Eq. (14), confirm that the entire families of the fundamental and twisted solitons are stable, see examples of the stability test in Figs. 3(b) and (f).

For  $g_0 = 0$ , a simple analysis of Eq. (19) demonstrates that  $\mu$  scales as  $r_0^{-2}$ , whereas the effective self-trapping size,  $r_0$  (provided that it is essentially larger than the transverse thickness,  $\varepsilon$ ), scales with the total norm,  $P$ , exactly as in Eq. (25). From here, the following scaling can be predicted for  $\alpha = 4$  and  $g_0 = 0$ :

$$\mu(g_0 = 0) \sim P^{\frac{2}{2\alpha-1}} \equiv P^{2/7}, \quad (27)$$

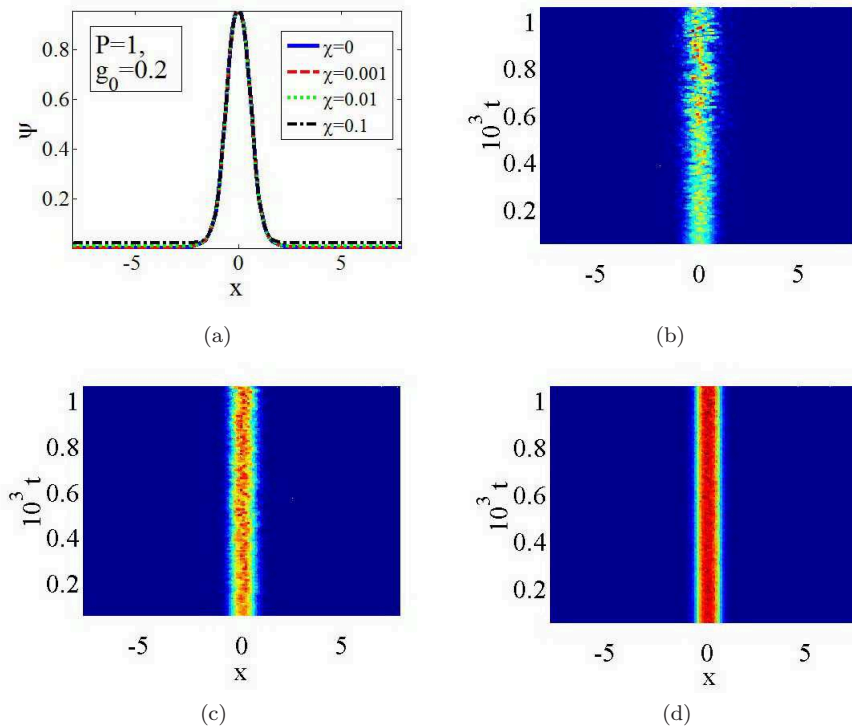


FIG. 2: (Color online) (a) Self-trapped modes found for different values of strength  $\chi$  of the expulsive potential (7), as indicated in the panel, for scaled norm  $P = 1$  and  $g_0 = 0.2$  in Eq. (26). Perturbed evolution of the self-trapped modes is shown in panel (b) for  $P = 0.1$ , in (c) for  $P = 1$ , and in (d) for  $P = 5$ . In the latter three panels,  $\chi = 0.1$  and  $g_0 = 0.2$ . The evolution is unstable for the weakly and moderately nonlinear modes in (b,c), and stable for the strongly nonlinear one in (d).

which pertains to the fundamental and twisted modes alike, and is quite close to the scaling exponent,  $\approx 1/3$ , found as the best fit of the numerically found dependences,  $\mu(P)$  (for both the fundamental and twisted solitons), to power-law functions in Figs. 3(c) and 3(g). This scaling is specific to the solitons in the nonlocal model, while in the local one it is completely different,  $\mu \sim P$ , for  $D = 1$  and 2 alike [45].

The presence of  $g_0 > 0$  in Eq. (26) does not affect very broad solitons corresponding to small  $P$ , hence the curves corresponding to  $g_0 = 0$  and  $g_0 = 0.2$  in Figs. 3(c) and 3(g) start from the same point at the smallest value of  $P$ . On the other hand, for narrow solitons with large  $P$ , one can still use the asymptotic equation (22) for the soliton's tail (at  $|x| \rightarrow \infty$ ), while inside the integral one may substitute  $g(x) \approx g_0$ , as suggested by Eq. (26). This means that, for the narrow solitons, scaling relations are obtained in the form of Eqs. (25) and (27), but with  $2\alpha$  replaced by  $\alpha$ . In particular, for  $\alpha = 4$  Eq. (27) is replaced by

$$\mu(g_0 > 0) \sim P^{\frac{2}{\alpha-1}} \equiv P^{2/3}, \quad (28)$$

which is reasonably close to the empirically found fitting exponent  $5/6$  quoted in Figs. 3(c) and 3(g).

As mentioned above, the derivation of the scaling relations (27) and (28) does not depend on the type of the self-trapped mode (fundamental/twisted), in agreement with the numerical results presented in Figs. 3(c) and 3(g). Higher-order multipole modes, which are not considered here, are expected to feature the same scaling too. On the other hand, the local model with the spatially growing strength of the self-repulsion [45, 46] suggests that instability may appear in families of higher-order modes.

Further, Figs. 3(d) and 3(h) show that, quite naturally, the spatial size of the fundamental and twisted modes decreases with the increase of the total norm, cf. Eq. (25). In this connection, Eq. (25) predicts, for  $\alpha = 4$ ,  $A_{\text{eff}} \sim P^{-1/7}$  in 1D, which is in accordance with the empirically found scaling exponents in Figs. 3(d) and 3(h).

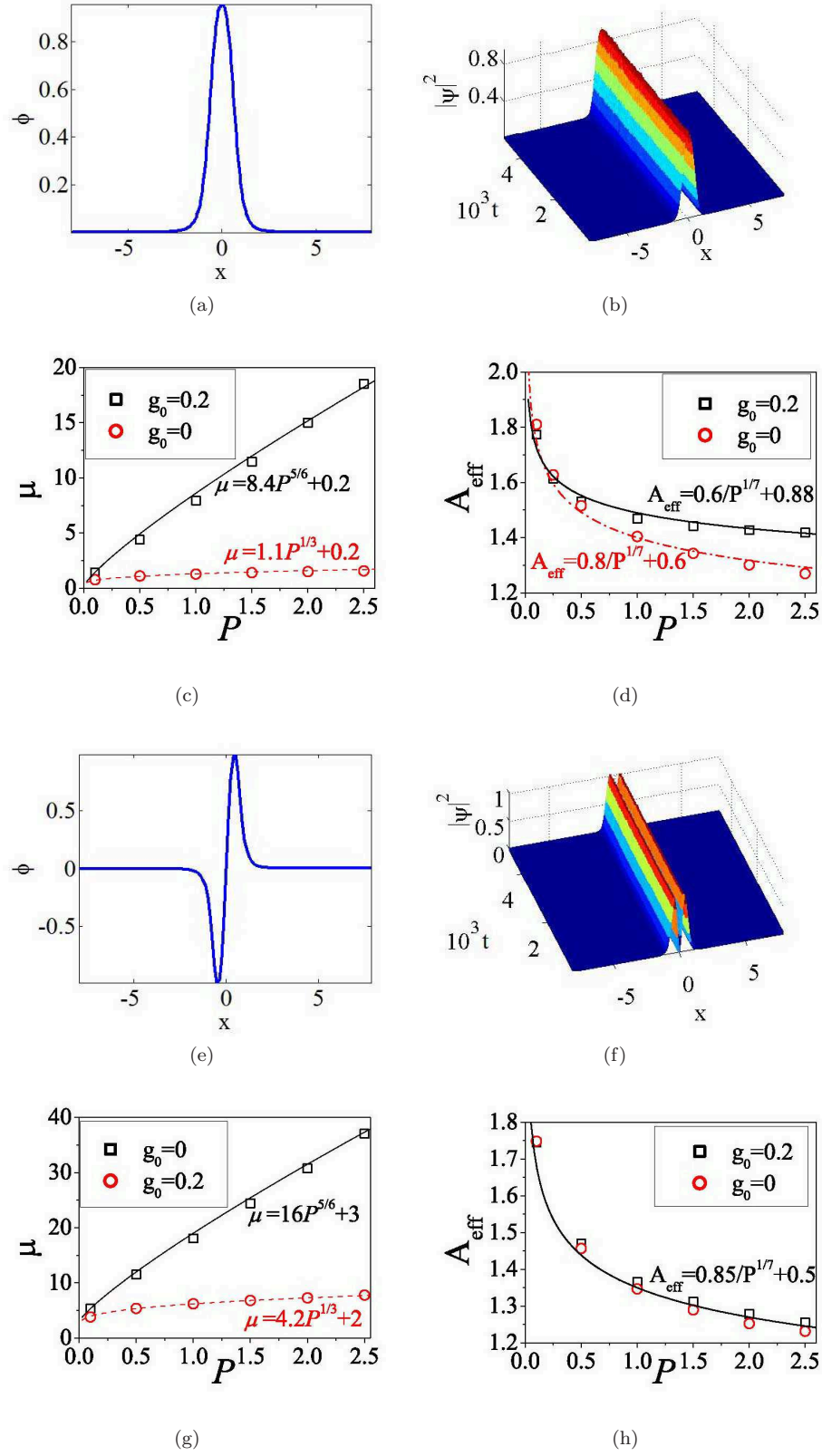


FIG. 3: (Color online) (a) An example of a 1D fundamental soliton with  $P = 1$  and  $g_0 = 0.2$ . (b) Stable perturbed evolution of this soliton. (c) The chemical potential versus the total norm for 1D fundamental-soliton families with different values of  $g_0$  [see Eq. (21)]. (d) The spatial width,  $A_{\text{eff}}$ , defined by the 1D counterpart of expression (20), versus  $P$  for the same families of the fundamental solitons. In panel (c), continuous curves display a fit of the numerical results to power-law approximations. (e)-(h) The same as in panel (a)-(d), but for twisted 1D solitons. In particular, panel (e) pertains to  $P = 1$  and  $g_0 = 0.2$ .



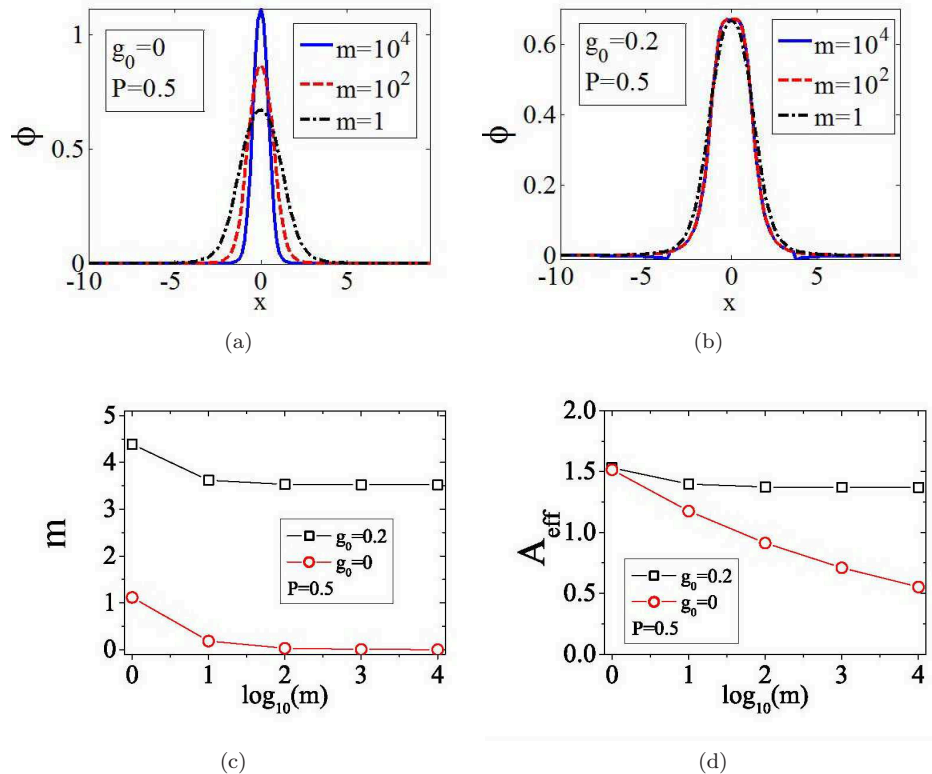


FIG. 4: (Color online) (a) Profiles of 1D fundamental solitons for a gradually increasing mass parameter,  $m$  [see Eq. (19)], and  $g_0 = 0$ . (b) The same for  $g_0 = 0.2$ . (c,d) The chemical potential and spatial size of the soliton versus  $m$  for different values of  $g_0$ . The case of large  $m$  represents the Thomas-Fermi approximation in the model with the long-range interactions.

### C. The Thomas-Fermi approximation for 1D fundamental solitons

As said above, the TFA very accurately predicts properties of fundamental solitons self-trapped in the model with the local strength of the self-repulsive contact nonlinearity growing as  $r^\alpha$  [45]. This fact suggests to try the same approximation in the present model, which implies the consideration of the limit of  $m \rightarrow \infty$  in Eq. (19). Unlike the local case, the TFA for the nonlocal equation cannot be solved analytically.

Figure 4 shows a set of profiles of 1D fundamental solitons, produced by the numerical solution of Eq. (19) for increasing  $m$ , at different values of  $g_0$ , along with the chemical potential and effective size of the solitons as functions of  $m$ . The results demonstrate that the TFA is very accurate at  $g_0 > 0$ , but it fails for  $g_0 = 0$ . This conclusion is not surprising, as the validity of the TFA is predicated on the presence of a nonvanishing self-repulsive nonlinearity.

### D. Numerical results for two-dimensional solitons

Similar to the 1D case, the numerical solution of the 2D equation (19) was at first performed taking into regard the EP,  $\chi > 0$ . As Fig. 5 shows, it has been concluded that, like in the 1D model, the 2D modes with a sufficiently strong nonlinearity remain robust, in agreement with the estimates presented at the end of Section I, while weakly unstable modes are subject to strong instability.

Further, Eq. (19) with  $\chi = 0$  reveals families of stable fundamental and vortical 2D solitons, which are displayed in Fig. 6. Note that panel 6(b) shows the TFA for the 2D fundamental soliton, with a flat area at the center, which is a typical feature of that approximation.

The vortices are produced, as usual, by the substitution of  $\phi(r, \theta) = \Phi(r) \exp(iS\theta)$  in Eq. (19), where  $(r, \theta)$  are the polar coordinates in the 2D plane,  $\Phi(r)$  is a real amplitude function, and  $S$  is integer vorticity (we here consider only  $S = 1$ ). Note that the asymptotic approximation (23) applies, at  $r \rightarrow \infty$ , to the vortices as well as to the 2D fundamental solitons.

The effective scaling of dependences  $\mu(P)$  for  $g_0 = 0$  in Figs. 6(c) and 6(g), as well as the scaling for narrow solitons

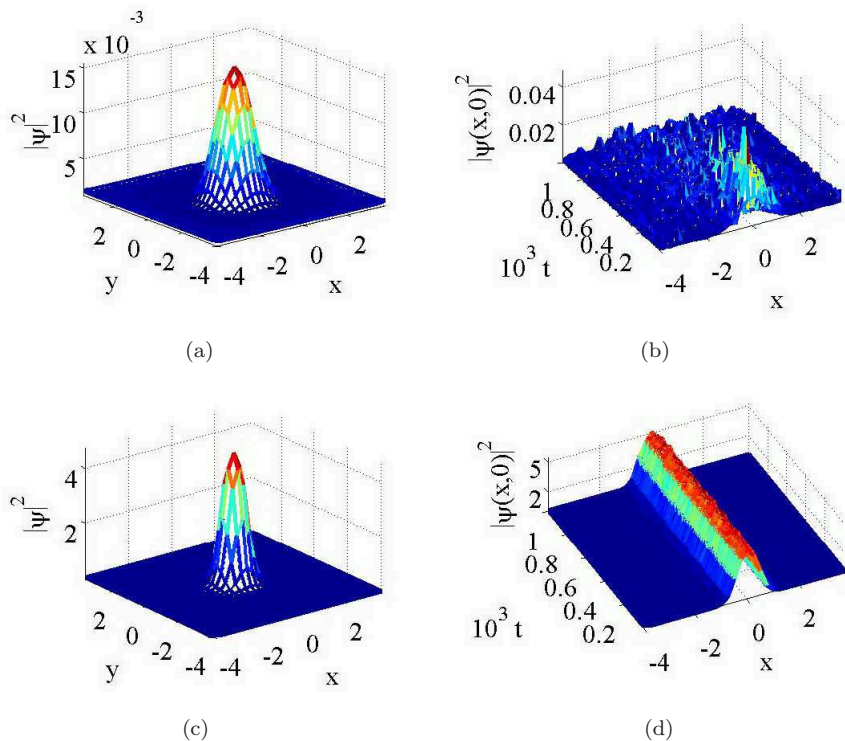


FIG. 5: (Color online) (a) The 2D self-trapped mode with  $\chi = 0.1$ ,  $P = 0.1$ , and  $g_0 = 0.2$ . (b) Completely unstable perturbed evolution of the mode from panel (a). (c) A strongly nonlinear 2D mode with  $\chi = 0.1$ ,  $P = 5$ , and  $g_0 = 0.2$ . (d) Stable perturbed evolution of the mode from panel (c).

(large  $P$ ) in the case of  $g_0 > 0$  in Eq. (21), which is also presented in Figs. 6(c) and 6(g), is explained by the same relations (27) and (28) which were derived above for the 1D case, as the derivation produces the results which do not depend on the dimension (the dimension cancels out in the process of the derivation), nor on the type of the soliton (fundamental or vortical). In addition to that, a straightforward analysis of the scaling for the effective area of the 2D solitons yields  $A_{\text{eff}} \sim P^{-2/7}$ , which also agrees well with the empiric scaling exponents indicated in Figs. 6(d) and 6(h).

Numerical tests of the perturbed evolution demonstrate that both the fundamental and vortex soliton families are entirely stable. Comparison to the model with the spatially modulated coefficient in front of the local self-defocusing term [45, 46] suggests that instability may arise for higher-order vortices. This issue is beyond the scope of the present work.

### III. MOBILITY OF THE FUNDAMENTAL SOLITONS

As well as in the model with the spatially modulated strength of the repulsive local nonlinearity [46], it is relevant to consider motion of stable solitons, which can be naturally initiated by a sudden shift of the soliton from the central position, and/or by kicking it. In this section, we study oscillatory and elliptic motion of 1D and 2D solitons, respectively, in the absence of the EP in Eq. (14),  $\chi = 0$ .

#### A. The 1D motion: Oscillations and destruction of the soliton

In the 1D case, the motion of the fundamental soliton was initiated by a shift ( $x_0$ ), which corresponds to initial condition  $\psi(x, t = 0) = \phi(x + x_0)$ . Figure 7 displays generic examples of the subsequent evolution of the shifted solitons, for different values of  $g_0$ . In Figs. 7(a) and 7(b), pertaining to  $g_0 = 0$ , the soliton initially compresses itself, and then approximately keeps its shape, performing undamped, although apparently irregular, oscillations around the center. In Figs. 7(c) - 7(h) corresponding to  $g_0 \neq 0$  ( $g_0 = 0.2, 0.4, \text{ and } 0.8$ ), the frequency of the oscillatory motion

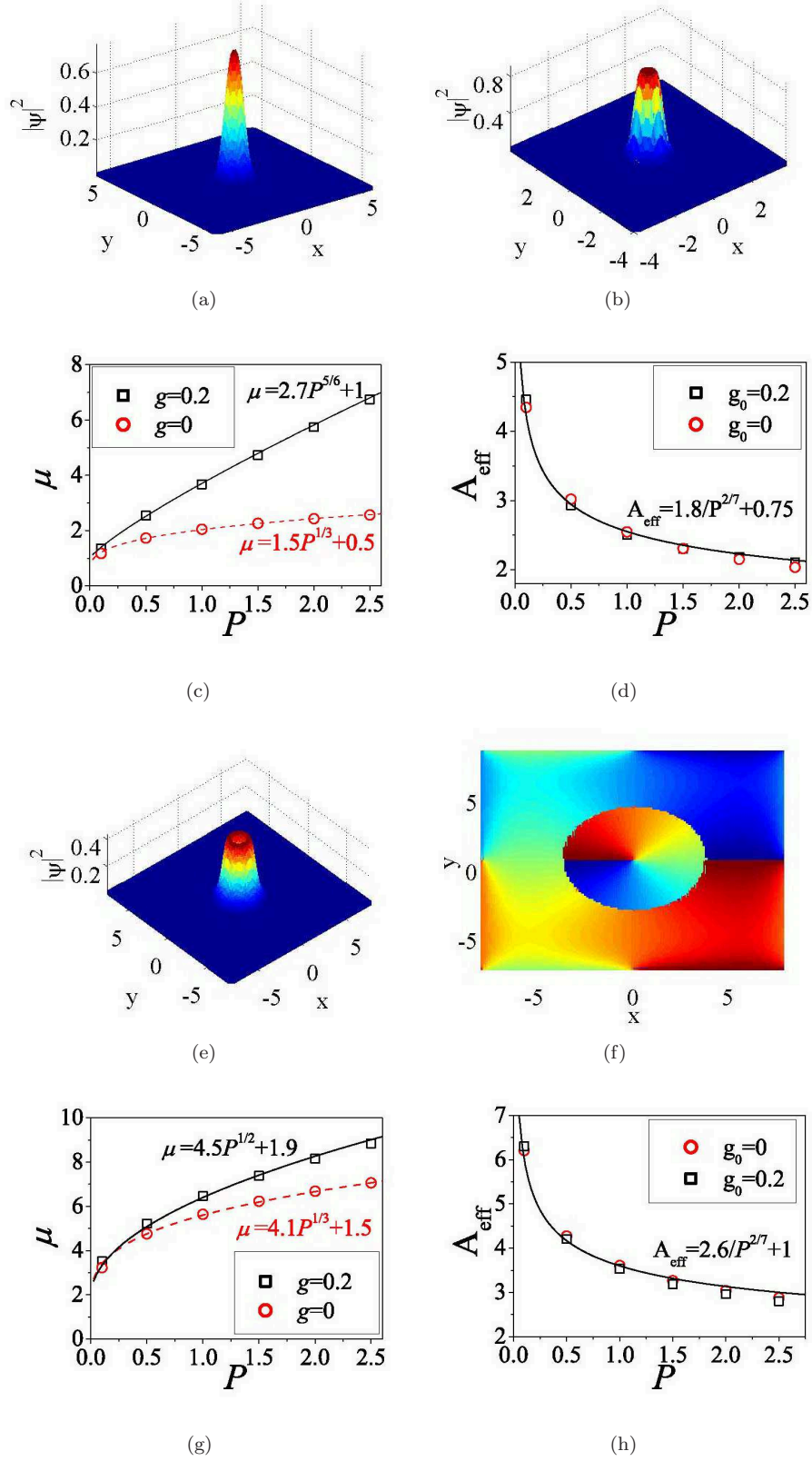


FIG. 6: (Color online) 2D self-trapped modes obtained in the model without the expulsive potential [ $\chi = 0$  in Eqs. (14) and (19)]. (a) An example of the 2D fundamental soliton with  $P = 1$  and  $g_0 = 0.2$ . (b) The Thomas-Fermi approximation for the same soliton, obtained from Eq. (19) with  $m = 10^4$ . (c) The chemical potential of the fundamental 2D solitons versus their total norm at different values of  $g_0$ . (d) The effective soliton's area  $A_{\text{eff}}$  [see Eq. (20)] versus the total norm for different values of  $g_0$ . (e) The amplitude profile of the 2D vortex soliton for  $P = 1$ ,  $g_0 = 0.2$ , and vorticity  $S = 1$ . (f) The phase distribution in this vortex. (g) The chemical potential of the vortex-soliton family versus the total norm for different values of  $g_0$ . (h) The effective area,  $A_{\text{eff}}$ , versus the total norm for the same families of vortical solitons.

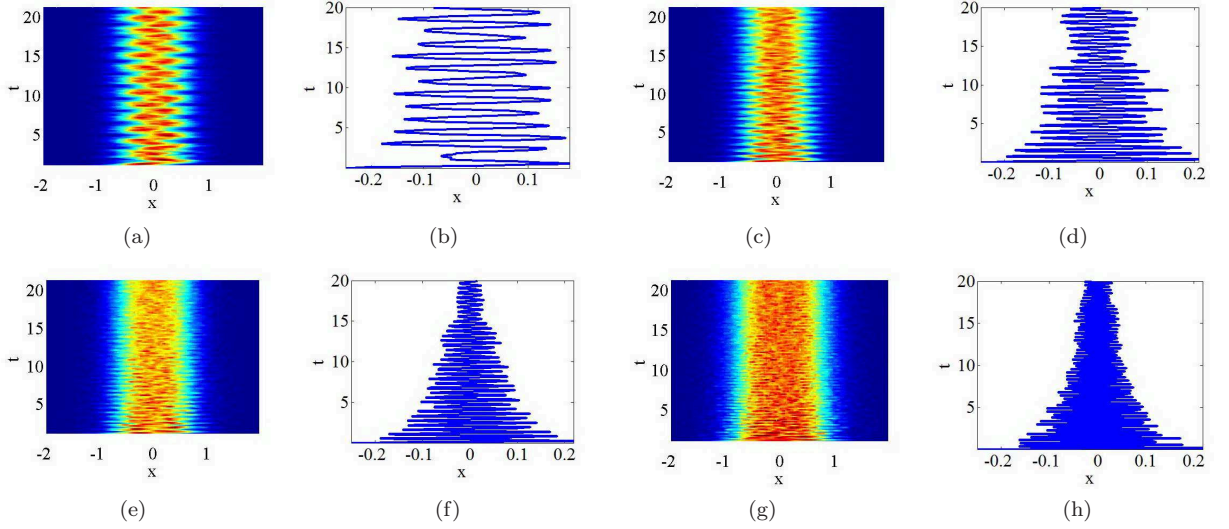


FIG. 7: (Color online) The evolution of a 1D fundamental soliton with  $P = 1$  and  $\chi = 0$ , which was initially shifted off the center by  $x_0 = 0.25$ . Panels (a), (c), (e) and (g) display top views of the evolution for  $g_0 = 0, 0.2, 0.4$  and  $0.8$ , respectively. Panels (b), (d), (f) and (h) are the center-of-mass trajectories of the moving solitons from panels (a), (c), (e) and (g), respectively, with the center-of-mass coordinate defined as  $x(t) \equiv P^{-1} \int_{-\infty}^{+\infty} x |\psi(x, t)|^2 dx$ .

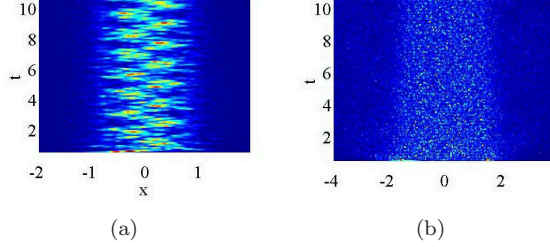


FIG. 8: (Color online) (a) The evolution of the 1D fundamental soliton with  $P = 1$  and  $g_0 = 0$ , which was initially shifted off the center by  $x_0 = 0.625$ . (b) Destruction of the soliton following the initial shift by  $x_0 = 1.5$ .

increases with  $g_0$ , while the amplitude of the center-of-mass oscillations gradually decreases, and the soliton suffers a slow decay, in the course of the evolution. The oscillating soliton features a gradual decay too with the increase of the initial shift, see an example in Fig. 8(a). Eventually, the soliton is quickly destroyed if the initial shift exceed a certain critical value, as shown in Fig. 8(b).

### B. The motion of 2D solitons: spiral trajectories

In the 2D case, one may expect the motion of a soliton, considered as a quasi-particle, along an elliptic trajectory, which can be initiated by shifting the soliton from the center along the  $x$ -direction (by distance  $x_0$ ), and simultaneously kicking it (in other words, imparting some velocity,  $\eta$ ) in the  $y$ -direction, i.e., setting  $\psi(\mathbf{r}, t = 0) = \phi(\mathbf{r} - \mathbf{x}_0)e^{i\eta y}$ . Figures 9 and 10 show results of the simulations at different values of  $x_0$  and  $\eta$ .

Similar to the 1D case, the moving soliton maintains its shape for small  $x_0$  and  $\eta$ , but splits into fragments if either  $x_0$  or  $\eta$  becomes too large. Therefore, we here discuss in detail only the case of small  $x_0$  and  $\eta$ . Figures 9 and 10 show results of such simulations for  $g_0 = 0$  and  $0.2$ .

As well as in the 1D setting,  $g_0$  strongly affects the motion. In Fig 9, panels (a)-(g) show that, at  $g_0 = 0$ , the soliton keeps its shape and follows a stable elliptic trajectory for a relatively long time, see panel 9(i). On the other hand, for  $g_0 = 2$  Fig. 10(i) demonstrates that the soliton's trajectory is an inward-winding spiral, rather than a closed ellipse, and in this case the 2D soliton relatively quickly returns to the center.

The soliton which has returned to the central position maintains *differential rotation* in its outer layer, which is

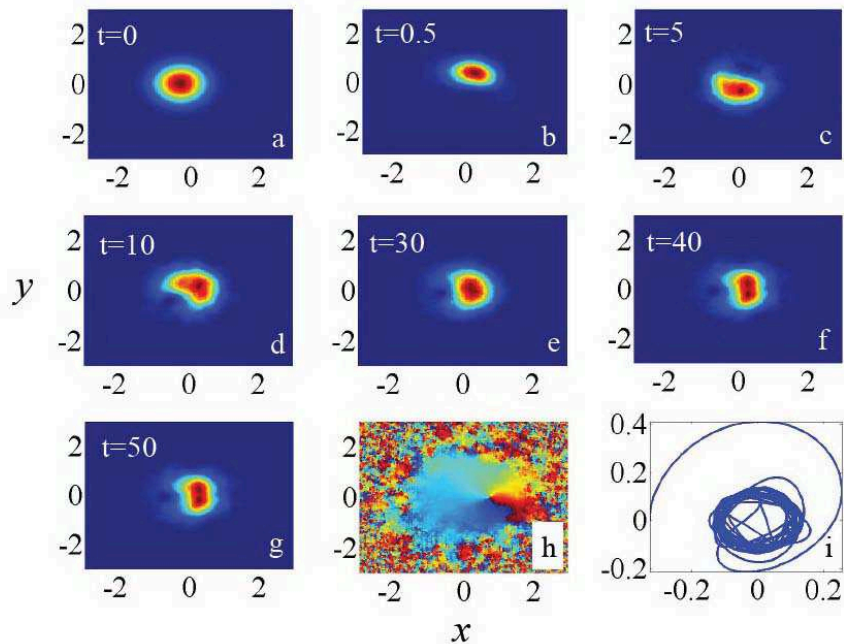


FIG. 9: (Color online) The evolution of the 2D fundamental soliton (for  $P = 1$ ,  $g_0 = 0$ ,  $\chi = 0$ ) initially shifted by  $x_0 = 0.3$  in the  $x$ -direction, and kicked in the  $y$ -direction by factor  $\exp(i\eta y)$ , with  $\eta = 2$ . Panels (a)-(g) display snapshots of the amplitude distribution at indicated moments of time. Panel (h) additionally displays the phase distribution at the last moment of time shown,  $t = 50$ . Panel (i) is the trajectory of the soliton's center of mass over the time interval  $0 \leq t \leq 50$ . The definition of the center-of-mass' position is  $\{x(t), y(t)\} = P^{-1} \int \int \{x, y\} |\psi(x, y, t)|^2 dx dy$ .

necessary to conserve the angular momentum lent to the system by the initial kick. This vortical structure exists without appearance of a zero density at the center [see Fig. 10(g) and 10(h)], which resembles known regimes of the differential rotation in superfluids, see, e.g., Ref. [67].

#### IV. THE DOUBLE-WELL NONLINEAR POTENTIAL

A natural generalization of the single-well modulation profile (26) is a double-well profile. In the 1D setting, it can be defined as

$$g(x) = (x^2 - \sqrt{g_0})^2, \quad (29)$$

with two minima set at  $x = \pm g_0^{1/4}$ , where  $g(x)$  vanishes. An incentive for the study of this modulation shape is search for a possibility of the spontaneous symmetry breaking between portions of the mean-field wave function trapped in the two symmetric nonlinear potential wells, and also a possibility of Josephson oscillations between them [68]. Here we briefly report results of this analysis performed in the framework of 1D equation (14) with  $\chi = 0$ .

Numerical computations yield stable even and odd states trapped in the double-well modulation profile (29). Typical examples of such localized modes are shown in Fig. 11. The comparison of the corresponding values of Hamiltonian (12), as a function of parameter  $g_0$  in Eq. (29), is shown in Fig. 12(a). It is concluded that the even mode represents the ground state, as it corresponds to a minimum of the Hamiltonian, although the energies of the two states become practically equal when  $g_0$  exceeds a certain critical value,  $g_0^c$ , see Fig. 12(a). The dependence of  $g_0^c$  on the total norm  $P$  is displayed in Fig. 12(b).

Within the explored parameter region, no stationary states with broken symmetry (or broken antisymmetry) have been found. On the other hand, robust but seemingly irregular Josephson oscillations can be readily initiated by placing the original matter-wave packet into one well. A typical example of robust oscillations is displayed in Fig. 13.

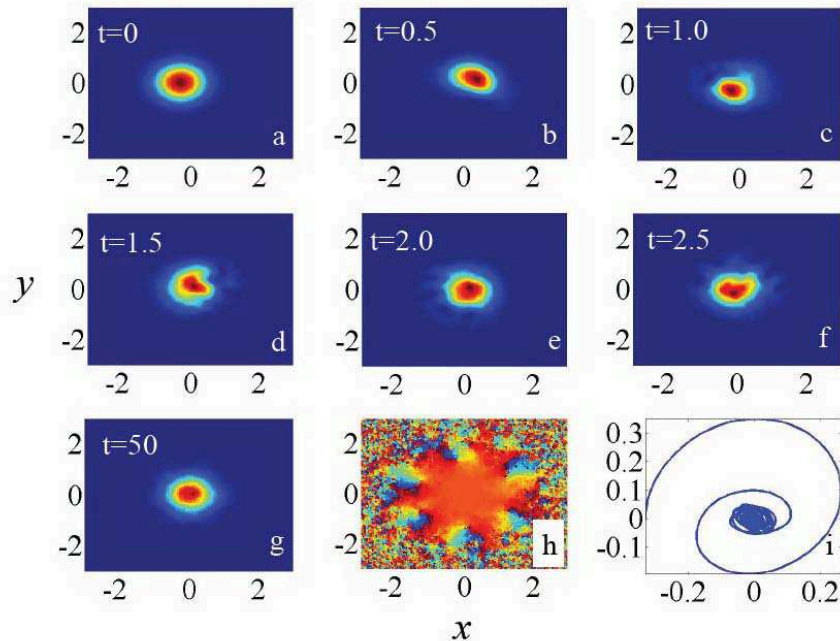


FIG. 10: (Color online) The same as in Fig. 9, but for  $g_0 = 0.2$ .

## V. CONCLUSION

The objective of this work is to explore possibilities for the formation of 1D and 2D fundamental solitons and solitary topological modes in the condensate of dipoles induced by spatially inhomogeneous polarizing fields. Under physically relevant conditions, this can be realized as self-trapping of bright solitons and vortices under the action of repulsive DDIs (dipole-dipole interactions) between the induced dipoles. Motivated by the recent analysis reported for the model with contact repulsive interactions [45]-[48], we have demonstrated that this counter-intuitive result is possible if the local dipole moment of particles, induced by the external fields perpendicular to the plane in which the condensate is trapped grows from the center to periphery faster than  $r^3$ , for both dimensions  $D = 1$  and  $2$  (unlike the local model, where the growth rate must be faster than  $r^D$ ). The setting also includes the EP (expulsive potential), due to the interaction of the induced dipoles with the polarizing field. The EP can be eliminated by choosing an appropriate relation between the dc and ac components of the field. Physical parameters have been estimated for the realization of the setting by means of the electric field. For modulation profile (21) with  $\alpha = 4$ , families of fundamental 1D and 2D solitons, 1D dipole modes, and 2D vortices have been found in a numerical form, and their scaling properties, which are essentially different from what was found recently in the local models, were explained analytically. It has also been demonstrated that the 1D and 2D fundamental solitons remain robust in the presence of the EP, provided that it is not too strong. The families of the trapped modes considered here are entirely stable if the EP is eliminated. In addition, the TFA (Thomas-Fermi approximation) was developed for the 1D and 2D fundamental solitons. The character of the solitons' confinement is opposite to the character of the repulsive nonlinearity: in the nonlocal model, the solitons are self-trapped tightly (super-exponentially), while the self-trapping in the local model is loose (algebraic).

A fundamental 1D soliton, shifted from the center, performs persistent oscillations if the initial shift is small enough, while a large shift can destroy it. Similarly, shifted and transversely kicked 2D solitons may feature persistent motion along elliptic trajectories. The 1D double-well modulation profile was considered too. In this case, both symmetric and antisymmetric trapped modes are dynamically stable, the symmetric ones realizing the ground state. In addition to that, the double-well structure readily supports persistent, although irregular, Josephson oscillations between the wells.

As an extension of this work, it may be interesting to study higher-order (multipole) modes in the 1D setting, and higher-order vortices in 2D. The effect of the EP on the twisted and vortical modes may be interesting too. Another relevant extension may deal with the interplay of the modulated repulsive DDIs and contact interactions. Furthermore, it should be quite interesting to study patterns supported by spatially periodic modulations of the polarizing field, which may be a specific ramification of the general concept of nonlinear lattices which, thus far, were

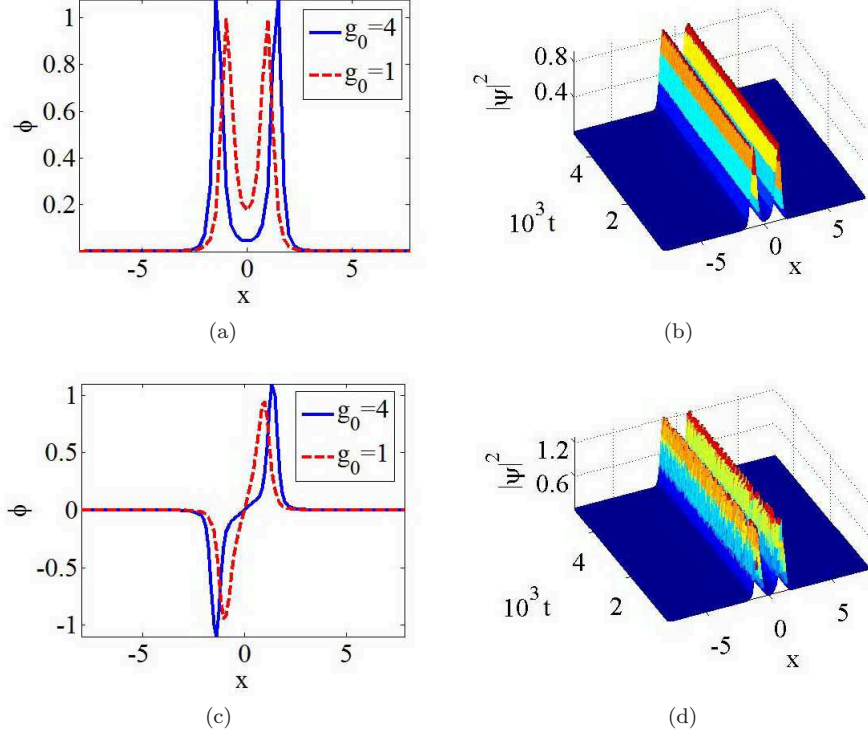


FIG. 11: (Color online) (a) Examples of stable even (symmetric) 1D solitons in the model with the double-well modulation function (29), for  $P = 1$ ,  $\chi = 0$ , and  $g_0 = 1$  or  $4$ . (b) Simulations of the perturbed evolution of the even soliton with  $g_0 = 1$ . (c) Stable odd (antisymmetric) solitons with  $P = 1$  and  $g_0 = 1$  or  $4$ . (d) Simulations of the perturbed evolution of the odd soliton with  $g_0 = 1$ .

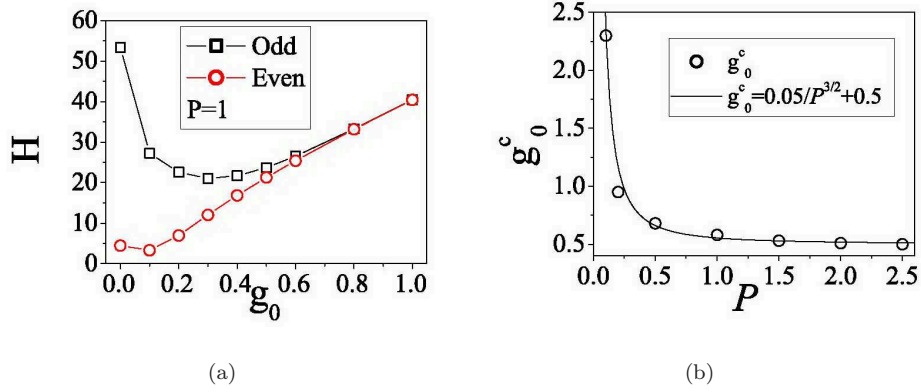


FIG. 12: (Color online) (a) The Hamiltonian (energy) of the even and odd 1D modes, trapped in the double-well modulation profile (29), versus  $g_0$ , for a fixed value of the total norm ( $P = 1$ ). (b) The degeneration point,  $g_0^c$ , at which energies of the even and odd norms become virtually equal, as a function of  $P$ . The inset indicates a fit of the dependence to a power-law approximation.

considered only in local systems [69], except for very recent work [70], where bright solitons were predicted in the 1D condensate of permanent dipoles under the external field periodically changing its orientation along the coordinate.

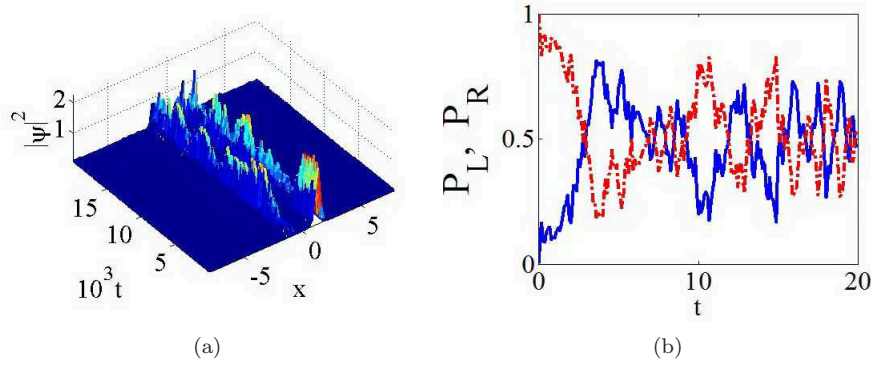


FIG. 13: (Color online) Irregular Josephson oscillations, initiated by a 1D wave packet originally placed around one minimum of the double-well modulation profile (29), with  $\chi = 0$ . (a) Results of the simulations initialized by  $\psi(x, t=0) = \sqrt{2} \operatorname{sech}\left(4\left(x - g_0^{1/4}\right)\right)$ , with  $g_0 = 2$  and total norm  $P = 1$ . (b) The corresponding evolution of the half-norms,  $P_L = \int_{-\infty}^0 |\psi|^2 dx$  and  $P_R = \int_0^{+\infty} |\psi|^2 dx$ .

### Acknowledgments

This work was supported by Chinese agency CNNSF (grants No. 11104083, 11204089, 11205063), by the German-Israel Foundation through grant No. I-1024-2.7/2009, and by the Tel Aviv University in the framework of the “matching” scheme for a postdoctoral fellowship of Y.L.

- 
- [1] A. Griesmaier, J. Werner, S. Hensler, J. Stuhler, and T. Pfau, Phys. Rev. Lett. **94**, 160401 (2005).
  - [2] Q. Beaufils, R. Chicireanu, T. Zanon, B. Laburthe-Tolra, E. Marchal, L. Vernac, J. -C. Keller, and O. Gorceix, Phys. Rev. A **77**, 061601 (2008).
  - [3] M. Lu, N. Q. Burdick, S. H. Youn, B. L. Lev, Phys. Rev. Lett. **107**, 190401 (2011).
  - [4] K. Aikawa, A. Frisch, M. Mark, S. Baier, A. Rietzler, R. Grimm, and F. Ferlaino, Phys. Rev. Lett. **108**, 210401 (2012).
  - [5] H. L. Bethlem, G. Berden, and G. Meijer, Phys. Rev. Lett. **83**, 1558 (1999).
  - [6] H. L. Bethlem, G. Berden, F. M. H. Crompvoets, R. T. Jongma, A. J. A. Van Roij, and G. Meijer, Nature **406**, 491 (2000).
  - [7] J. R. Bochinski, E. R. Hudson, H. J. Lewandowski, G. Meijer and J. Ye, Phys. Rev. Lett. **91**, 243001 (2003).
  - [8] S. Y. T. van de Meerakker, P. H. M. Smeets, N. Vanhaecke, R. T. Jongma, and G. Meijer, Phys. Rev. Lett. **94**, 023004 (2005).
  - [9] A. Griesmaier, J. Phys. B: At. Mol. Opt. Phys. **40**, R91 (2007).
  - [10] T. Lahaye, C. Menotti, L. Santos, M. Lewenstein, and T. Pfau, Rep. Prog. Phys. **72**, 126401 (2009).
  - [11] Y. Kawaguchi, and M. Ueda, Phys. Rep. **520**, 253 (2012).
  - [12] H. Saito, Y. Kawaguchi, and M. Ueda, Phys. Rev. Lett. **102**, 230403 (2009).
  - [13] R. Nath, and L. Santos, Phys. Rev. A **81**, 033626 (2010).
  - [14] A. Maluckov, G. Gligorić, L. Hadžievski, B. A. Malomed, and T. Pfau, Phys. Rev. Lett. **108**, 140402 (2012).
  - [15] M. Klawunn, and L. Santos, Phys. Rev. A **80**, 013611 (2009).
  - [16] K. Lাকomy, R. Nath, and L. Santos, Phys. Rev. A. **86**, 023620 (2012).
  - [17] E. Wikberg, J. Larson, E. J. Bergholtz, and A. Karlhede, Phys. Rev. A. **85**, 033607 (2012).
  - [18] T. Lahaye, J. Metz, F. Fröhlich, T. Koch, M. Meister, A. Griesmaier, T. Pfau, H. Saito, Y. Kawaguchi, and M. Ueda, Phys. Rev. Lett. **101**, 080401 (2008).
  - [19] J. Metz, T. Lahaye, B. Fröhlich, A. Griesmaier, T. Pfau, H. Saito, Y. Kawaguchi, and M. Ueda, New J. Phys. **11**, 055032 (2009).
  - [20] M. Vengalattore, S. R. Leslie, J. Guzman, D. M. Stamper-Kurn, Phys. Rev. Lett. **100**, 170403 (2008).
  - [21] M. Fattori, G. Roati, B. Deissler, C. Derrico, M. Zaccanti, M. Jona-Lasinio, L. Santos, M. Inguscio, G. Modugno, Phys. Rev. Lett. **101**, 190405 (2008).
  - [22] S. E. Pollack, D. Dries, M. Junker, Y. P. Chen, T. A. Corcovilos, and R. G. Hulet, Phys. Rev. Lett. **102**, 090402 (2009).
  - [23] S. Müller, J. Billy, E. A. L. Henn, H. Kadau, A. Griesmaier, M. Jona-Lasinio, L. Santos, and T. Pfau, Phys. Rev. A **84**, 053601 (2011).
  - [24] J. Cuevas, B. A. Malomed, P. G. Kevrekidis, and D. J. Frantzeskakis, Phys. Rev. A **79**, 053608 (2009).
  - [25] K. Gawryluk, K. Bongs, and M. Brewczyk Phys. Rev. Lett. **106**, 140403 (2011).
  - [26] P. Hauke, F. M. Cucchietti, L. Tagliacozzo, I. Deutsch, and Lewenstein, Rep. Prog. Phys. **75**, 082401 (2012).



- [27] C. Conti, M. Peccianti, and G. Assanto, Phys. Rev. Lett. **92**, 113902 (2004).
- [28] W. Królikowski, O. Bang, N. Nikolov, D. Neshev, J. Wyller, J. J. Rasmussen, and D. Edmundson, J. Opt. B: Quantum Semiclass. Opt. **6**, S288 (2004).
- [29] A. S. Desyatnikov, D. N. Neshev, Y. S. Kivshar, N. Sagemerten, D. Träger, J. Jägers, C. Denz, and Y. V. Kartashov, Opt. Lett. **30**, 869 (2005).
- [30] S. Sinha, and L. Santos, Phys. Ret. Lett. **99**, 140406 (2007).
- [31] P. Pedri, and L. Santos, Phys. Rev. Lett. **95**, 200404 (2005).
- [32] I. Tikhonenkov, B. A. Malomed, and A. Vardi, Phys. Rev. A **78**, 043614 (2008).
- [33] V. M. Lashkin, Phys. Rev. A **75**, 043607 (2007).
- [34] I. Tikhonenkov, B. A. Malomed, and V. Vardi, Phys. Rev. Lett. **100**, 090406 (2008).
- [35] P. Köberle, D. Zajec, G. Wunner, and B. A. Malomed, Phys. Rev. A **85**, 023630 (2012).
- [36] R. Eichler, J. Main, and G. Wunner, Phys. Rev. A **83**, 053604 (2011).
- [37] R. Nath, P. Pedri, and L. Santos, Phys. Rev. Lett. **102**, 050401 (2009).
- [38] R. Nath, P. Pedri, and L. Santos, Phys. Rev. A **76**, 013606 (2007).
- [39] Y. Li, J. Liu, W. Pang, B. A. Malomed, Phys. Rev. A **87**, 013604 (2013).
- [40] Z. Luo, Y. Li, W. Pang, and Y. Liu, J. Phys. Soc. Jpn. **82** 094401 (2013).
- [41] B. B. Baizakov, F. Kh. Abdullaev, B. A. Malomed, and M. Salerno, J. Phys. B: At. Mol. Opt. Phys. **42**, 175302 (2009).
- [42] K. E. Strecker, G. B. Partridge, A. G. Truscott, and R. G. Hulet, New J. Phys. **5**, 731 (2003).
- [43] V. A. Brazhnyi, and V. V. Konotop, Mod. Phys. Lett. B **18**, 627 (2004).
- [44] F. K. Abdullaev, A. Gammal, A. M. Kamchatnov, and L. Tomio, Int. J. Mod. Phys. B **19**, 3415 (2005).
- [45] O. V. Borovkova, Y. V. Kartashov, B. A. Malomed, and L. Torner, Opt. Lett. **36**, 3088 (2011).
- [46] O. V. Borovkova, Y. V. Kartashov, L. Torner, and B. A. Malomed Phys. Rev. E **84**, 035602(R) (2011).
- [47] Y. V. Kartashov, V. A. Vysloukh, L. Torner, and B. A. Malomed, Opt. Lett. **36**, 4587 (2011).
- [48] V. E. Lobanov, O. V. Borovkova, Y. V. Kartashov, B. A. Malomed, and L. Torner, Opt. Lett. **37**, 1799 (2012).
- [49] J. Zeng and B. A. Malomed, Phys. Rev. E **86**, 036607 (2012).
- [50] Y. He and B. A. Malomed, Phys. Rev. A **87**, 053812 (2013).
- [51] B. A. Malomed, D. Mihalache, F. Wise, and L. Torner, J. Optics B: Quant. Semicl. Opt. **7**, R53 (2005).
- [52] S. Yi, and L. You, Phys. Rev. A **61**, 041604 (2000).
- [53] B. Deb, and L. You, Phys. Rev. A **64**, 022717 (2001).
- [54] T. J. McCarthy, M. T. Timko, and D. R. Herschbach, J. Chem. Phys. **125**, 133501 (2006).
- [55] Z. D. Li, Q. Y. Li, P. B. He, J. Q. Liang, W. M. Liu, and G. S. Fu, Phys. Rev. A **81**, 015602 (2010).
- [56] A. E. Golomedov, G. E. Astrakharchik, and Y. E. Lozovik, Phys. Rev. A **84**, 033615 (2011).
- [57] G. te Velde, F. M. Bickelhaupt, E. J. Baerends, C. Fonseca Guerra, S. J. A. Van Gisbergen, J. G. Snijders, and T. Ziegler, J. Comp. Chem. **22**, 931 (2001).
- [58] J. Moxom, P. T. A. Reilly, W. B. Whitten, and J. M. Ramsey, Rapid Comm. Mass Spectrometry **16**, 755 (2002).
- [59] M. Hellwig, A. Bautista-Salvador, K. Singer, G. Werth, and F. Schmidt-Kaler New J. Phys. **12**, 065019 (2010).
- [60] J. Zou, C. Liu, and J. E. Schutt-Ainé, Int. J. RF and Microwave Comp. Aided Eng. **11**, 322 (2001); J. Chen, J. Zou, C. Liu, J. E. Schutt-Ainé, and S.-M. Kang, IEEE Trans. Electr. Dev. **50**, 730 (2003); F. Najjar, S. Choura, S. El-Borgi, E. M. Abdel-Rahman, and A. H. Nayfeh, J. Micromech. Microeng. **15**, 419 (2005).
- [61] H. Sakaguchi, and B. A. Malomed, Phys. Rev. A **83**, 013907 (2011).
- [62] B. Arora, M. S. Safronova, and C. W. Clark, Phys. Rev. A **76**, 052516 (2007); S. Ospelkaus, K.-K. Ni, M. H. G. de Miranda, B. Neyenhuis, D. Wang, S. Kotochigova, P. S. Julienne, D. S. Jin, and J. Ye, Faraday Discuss. **142**, 351 (2009).
- [63] G. Kurizki, I. E. Mazets, D. H. J. O'Dell, and W. P. Schleich, Int. J. Mod. Phys. B **18**, 961 (2004).
- [64] J. Yang and T. I. Lakoba, Stud. Appl. Math. **118**, 153 (2007).
- [65] J. Yang and T. I. Lakoba, Stud. Appl. Math. **120**, 265 (2008).
- [66] H. Sakaguchi, and B. A. Malomed, Phys. Rev. A **81**, 013624 (2010).
- [67] D. M. Sedrakian, and B. Carter, Monthly Not. Roy. Astron. Soc. **297**, 1189 (1998).
- [68] B. A. Malomed (editor), *Spontaneous Symmetry Breaking, Self-Trapping, and Josephson Oscillations in Nonlinear Systems* [Springer-Verlag: Berlin and Heidelberg, 2013, ISBN 978-3-642-21206-2 ISBN 978-3-642-21207-9 (eBook)].
- [69] Y. V. Kartashov, B. A. Malomed, and L. Torner, Rev. Mod. Phys. **83**, 247 (2011).
- [70] F. Kh. Abdullaev, A. Gammal, B. A. Malomed, and L. Tomio, Phys. Rev. A **87**, 063621 (2013).